International Journal of Robotics and Control Systems
Vol. 4, No. 3, 2024, pp. 1304-1318
ISSN 2775-2658
http://pubs2.ascee.org/index.php/ijrcs

Study of the Crowbar's Functioning in Doubly Fed Induction Wind Generators: Towards Achieving Fault Ride Through Capability

Hashim Alnami [a,1,*]

[a] Department of Electrical and Electronic Engineering, College of Engineering and Computer Science, Jazan University, P.O. Box114, Jazan 45142, Saudi Arabia
[1] halnami@jazanu.edu.sa
* Corresponding Author

ARTICLE INFO

Article history
Received June 10, 2024
Revised July 13, 2024
Accepted July 28, 2024

Keywords
Crowbar;
Fault Ride Through Capability;
DFIG;
Wind Energy;
Protection Strategy

ABSTRACT

This work examines the analysis of temporary behaviors and crowbar hardware layout for enhancing the fault ride-through capability (FRTC) in doubly fed induction wind generators (DFIWGs) A crowbar that is linked in parallel to the rotor side converter (RSC) is a feature found on the majority of DFIWGs these days to safeguard the RSC and DC-bus capacitor (DCBC). Previous studies demonstrated that the crowbar resistance has an impact on the DFIWG transient response's oscillations and peak values. In order to satisfy the FRTC criterion, the article initially methodically examines the DFIWG dynamics with and without a crowbar during a 100% voltage dip and studies the effects of two resistance values on the DCBC. It has been demonstrated that choosing a crowbar resistance greater than the permitted range may cause the DFIG FRT performance to decline. By actively addressing grid faults and improving performance, stability, and dependability, this integrated crowbar shows the potential of state-of-the-art control approaches for the dependable and efficient use of DFIWGs. MATLAB/Simulink is used to run robust simulations, and the results unambiguously show that the proposed model may significantly improve the FRTC of DFIWGs.

1. Introduction

In the years to come, wind power is going to be significantly influenced by the sheer amount of wind systems (WSs) linked to the grid; therefore, more WSs will be needed to remain linked to the grid in the event of a fault. In order to ensure the reliability of the power system (PS), WSs must be able to assist in controlling the grid voltage throughout failures, a function known as fault ride-through capability (FRTC) [1]-[3]. Additionally, this is a necessary component of the WS grid code [4]-[6].

In many modern WS facilities, variable speed sort with power converters for control have been employed. Because of this, these kinds have the ability to control their own reactive power (Q) and run at unity power factor [7]-[11]. The DFIWG is currently the most popular one; Fig. 1 depicts a DFIWG's structure and control system. With this kind, the rotor's windings are supplied via bi-PWM voltage source converters (VSC), while the stator windings are linked straight to the grid. Put another

way, VSC links to the network and the rotor regulates a device. A portion of the machine's total power, roughly 30%, is intended to be transferred by the VSC [7], [12]-[14]. The speed range of the DFIWG is determined by the VSC's size. From the stator to the network, the RSC regulates the P and Q of WSs. In addition to allowing the VSC to produce or absorb Q, the grid side converter (GSC) regulates the DCBC [15]-[17]. The power can be supplied by the DFIWG's rotor and stator. On the other hand, the DFIWG speed and wind speed determine which way active electricity flows through the rotor circuit [18]. Due to its direct connection to the grid via the stator winding, the DFIWG's primary drawback is its susceptibility to power grid disturbances [19]-[21].

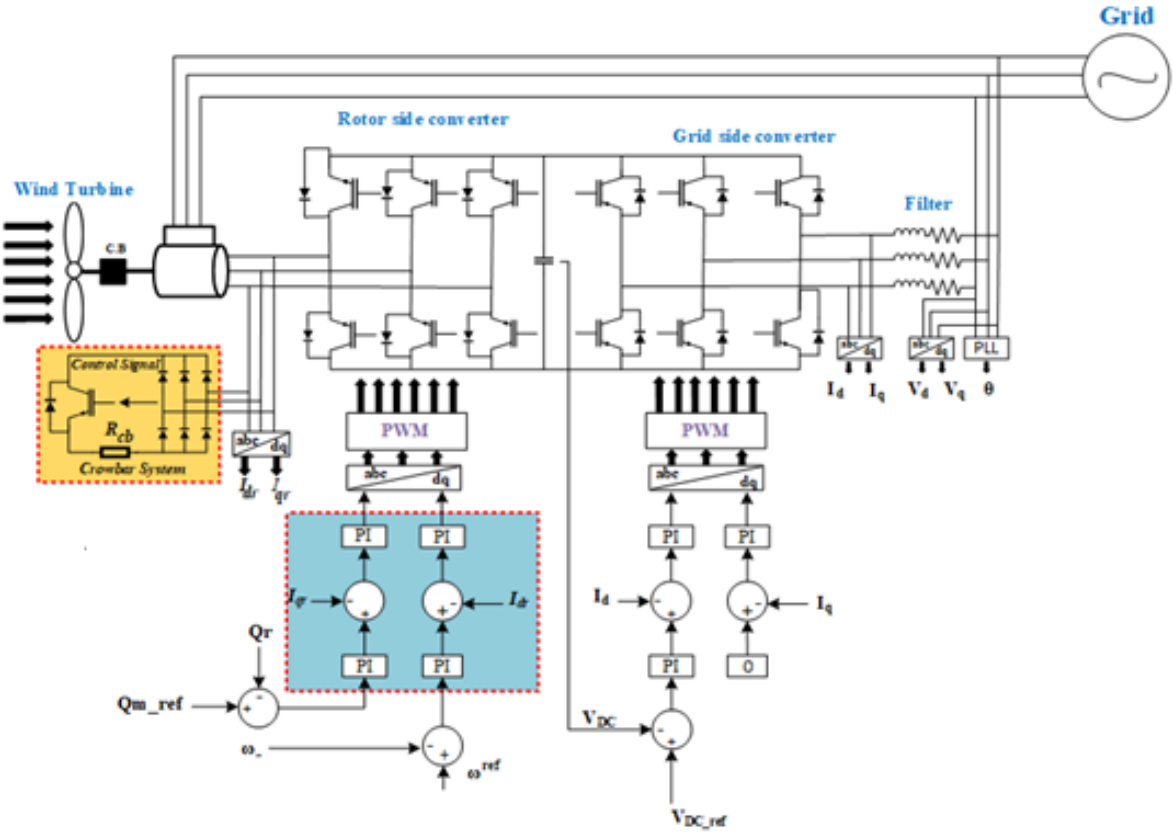

Fig. 1. Studied system

Active crowbar (ACR) is typically used to reduce the high currents during faults, improving the fault handling capability and shielding the DFIWG VSC from high rotor current. Where the VSCs are employed: in the rotor circuit. When an ACR is employed to briefly short-circuit the rotor in order to offer FRTC, the behavior of DFIWG was examined in [22], [23]. It was discovered that DFIWG permits the power grid's Q support even during fault situations, and this support is greater when the WS is not heavily loaded and when a voltage regulator is utilized in place of the DFIWG's continuous power factor management. In order to lessen unwanted fault effects, the ACR approach was implemented in [24], [25], helping to maintain grid voltage management during emergencies.

Since the DFIWG stator is physically linked to the network, any disruption in the electrical network can also generate a stator disruption, which can have a significant impact on the rotor, RSC, and DCBC. In [26], the impact of DCBC breakdown was examined in order to monitor the DFIWG parameter values in a WS. Nevertheless, no research was done on how one generator's DCB breakdown affected the efficiency of the other units in the WS bus bar. When power support (also referred to as the FRTC) fails, DFIWG can remain connected to the grid if the RSC has an ACR installed [27], [28]. Once the fault has been fixed, the GSC can once more be controlled to preserve the DCB voltage (DCBV). Nonetheless, there's a good chance that the DCBV will vary either throughout or afterward the defect is fixed. Ref., [29] suggested an enhanced control approach with

immediate rotary power feedback to restrict the DCBV oscillations for a VSC in a DFIWG. Two control actions can be used to enable the ACR to accomplish the FRTC at the time the fault happens [27], [30]. Unplugging the RSC from the rotor without unplugging the WS from the network is the first step. The DFIWG will function as an IM with a high rotor resistance in this scenario [31]. Maintaining the RSC's connection to the rotor and the WS's joining the network is the second approach. After the issue is cleared, a regular operation can be resumed right away with the help of this control action [32]. A summary of some of the published works is listed in Table 1.

Table 1. Comparison of previously published works in this field

Refs.	Converters		Role of study			Notes
	RSC	GSC	MPPT	PAC	FRTC	
[33]	✓	×	×	×	✓	The rotor circuit's transient current is decreased when feed-forward current regulation is applied when a malfunction happens quickly.
[34]	×	✓	×	×	✓	A dual vector and direct power controller are used to rapidly inject Q amid voltage dips and reduce the overcurrent in the rotor and stator.
[35]	✓	✓	✓	×	✓	A redesigned adaptive control system was introduced to the original standard vector control, and it proved useful in mitigating sensor malfunctions and ensuring acceptable response under faults.
[36]	×	×	×	×	✓	The outcomes demonstrated that SMC functions well in the presence of unexpected voltage drop levels and nonlinear dynamics.
[37]	×	×	×	×	✓	At the PCC, the dynamic adaptive multi-cell FCL topology was connected, greatly enhancing system performance and providing a flexible voltage dip correction methodology contingent on voltage levels. The effectiveness of the proposed technique was confirmed by comparative testing with the single-cell FCL.
[38]	✓	✓	✓	✓	×	After comparing the FLC, H infinity (H∞), and PI controllers' performances, it was found that H∞ performed the best where it provides improved performance and lower harmonics.
[39]	✓	×	✓	✓	×	The three controllers with the lowest tracking error—SM, PI, and advanced backstepping (AB)—were examined and their precision was evaluated. The fast reaction times and resilience were among the advantages of the ABC.

This study examines how the DFIWG behaves when the ACR is activated and deactivated. It also illustrates how the RSC and GSC control systems can improve the DCB reaction to assist the network throughout system disruptions by taking into account the worst-case scenarios of short circuits that could happen near the stator terminals. Additionally, this study looks into the resistance value's impact. This paper's remaining sections are arranged as follows. The modeling and control of the DFIWG parts have been briefly covered in Section 2. Section 3 provides information on the coordinated control strategy and how ACR operates. The results collected and the validation of the suggested approach are presented in Section 4. This paper is finally concluded in Section 5.

2. System Modelling

DFIWG is what nature uses. Typically, an electric control technique is used to ensure the rotor circuit, allowing for variable speed processes. According to Fig. 2 (a) and Fig. 2 (b), DFIWGs can operate in one of two ways: When the generator is operating in a super synchronous mode in the (i) Mode Nr > Ns, s is negative and both stator/rotor windings transmit energy from the grid. In the second mode Nr, Ns, s is $+^{tve}$ generator is operating in sub-synchronous mode, stator winding is supplying power from the rotor winding [41]-[43].

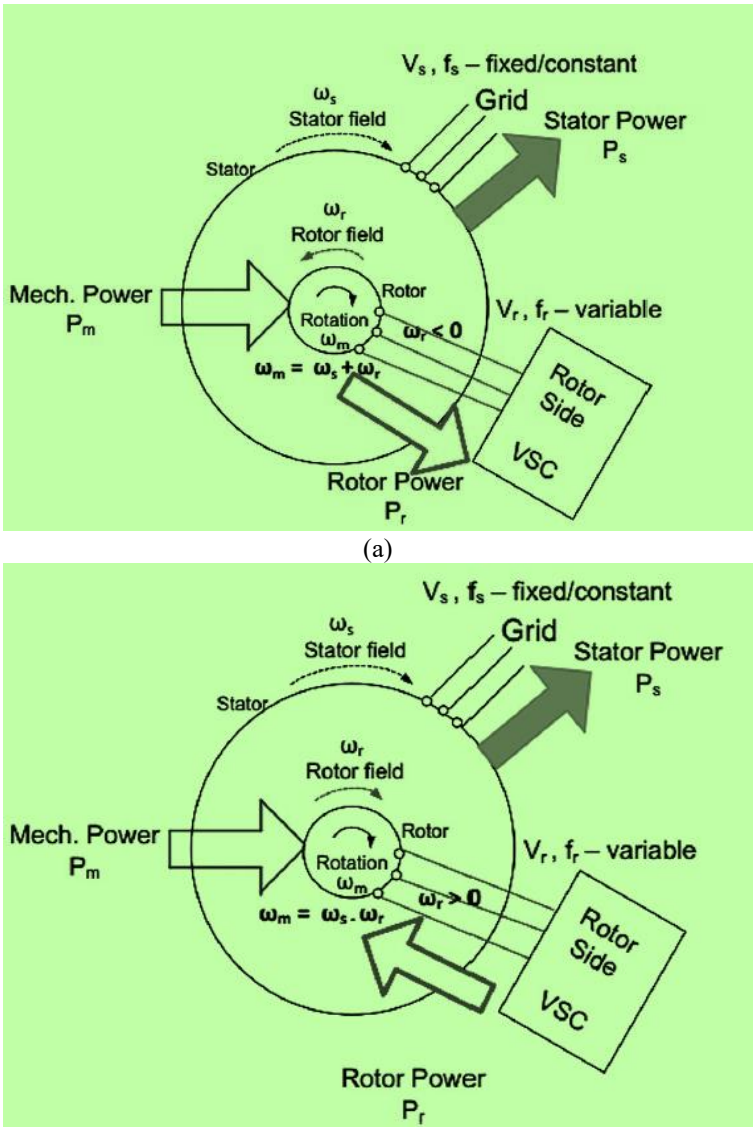

Fig. 2. DFIWG modes: (a) super-synchronous, (b) sub-synchronous

This section explains in detail the DFIWG mathematical modeling. There is access to the machine data as reactance per unit. Fig. 2 depicts the DFIWG equivalent circuit. The machine's equilibrium equations are therefore expressed as follows. The conventional following is the DFIWG's electrical equation in the park frame, which transforms the voltage equations to a synchronously rotating frame of reference [44], [45].

$$v_{qs} = r_s i_{qs} + \frac{\omega}{\omega_b}\psi_{ds} + \frac{p}{\omega_b}\psi_{qs} \quad (1)$$

$$v_{ds} = r_s i_{ds} + \frac{\omega}{\omega_b}\psi_{qs} + \frac{p}{\omega_b}\psi_{ds} \quad (2)$$

$$v_{0s} = r_s i_{0s} + \frac{p}{\omega_b}\psi_{qs} \quad (3)$$

$$v'_{qr} = r'_r i'_{0r} + \left(\frac{\omega - \omega_r}{\omega}\right)\psi'_{qr} + \frac{p}{\omega_b}\psi_{qr} \quad (4)$$

$$v'_{dr} = r'_r i'_{dr} + (\frac{\omega - \omega_r}{\omega})\psi'_{qr} + \frac{p}{\omega_b}\psi_{dr} \quad (5)$$

$$v'_{0r} = r'_r i'_{0r} + \frac{p}{\omega_b}\psi'_{0r} \quad (6)$$

Inductive reactance was calculated using the electrical basis angular velocity shown above. Following are the links between flux and volts per second. d-q frame depicts both the d-q-axis comparable circuit and control system schematic diagram shown in Fig. 3.

$$\psi_{qs} = X_{Is} i_{qs} + X_M(i_{qs} + i'_{qr}) \quad (7)$$

$$\psi_{ds} = X_{Is} i_{ds} + X_M(i_{ds} + i'_{dr}) \quad (8)$$

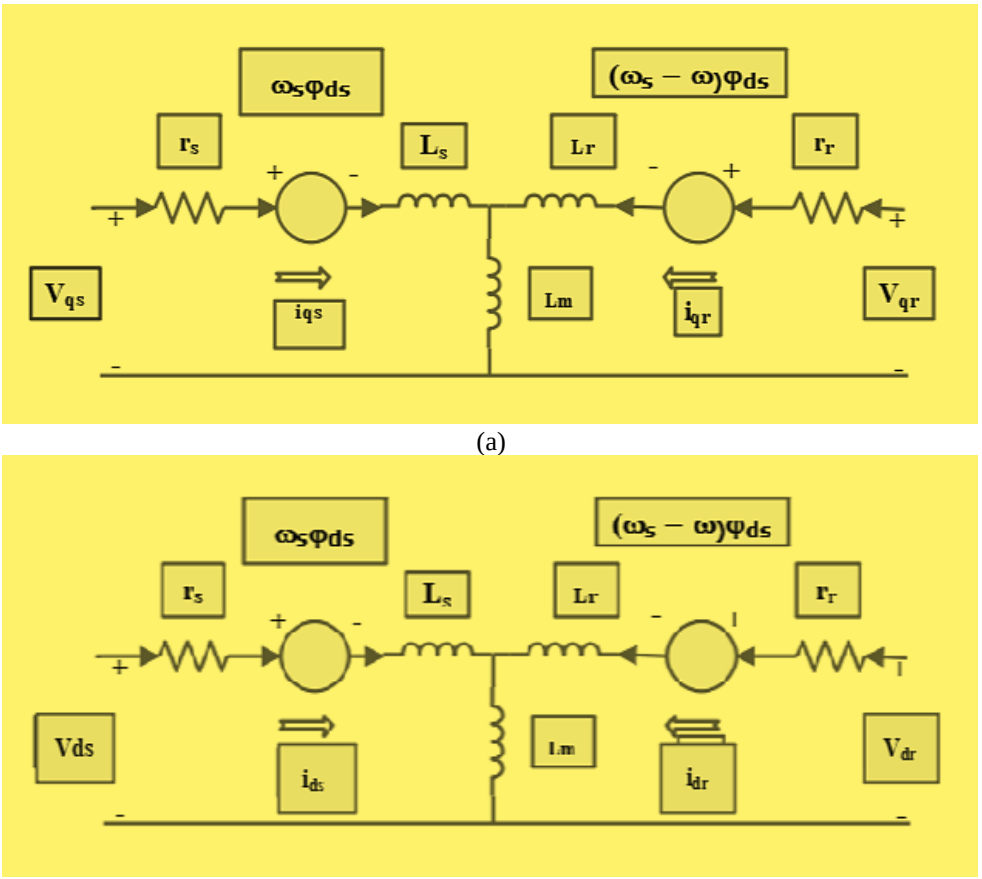

Fig. 3. (a) d-q frame depicts both the d-q-axis comparable circuit and (b) control system schematic diagram

$$\psi'_{0s} = X'_{Is} i_{0s} \quad (9)$$

$$\psi'_{qr} = X'_{Ir}{}' i_{qr} + X_M(i_{qs} + i'_{qr}) \quad (10)$$

$$\psi'_{dr} = X'_{Is} i'_{dr} + X_M(i_{ds} + i'_{dr}) \quad (11)$$

$$\psi'_{0r} = X'_{Is} i'_{0r} \quad (12)$$

By multiplying ω_b by inductance in the equations above, the inductive reactance is found. The voltage Eqs (3) through (11) deal with current and flux connections (per second). Because of their

interdependence, currents and flux connections cannot exist independently or as state variables. The desired outcomes are attained to describe the voltage Eqs involving either current or flux linkage during the development of transfer functions and compute modeling of DFIWG. The voltage equation changes to look like the following if the current is treated as an independent variable and flux connections are replaced with current.

$$\begin{bmatrix} v_{qs} \\ v_{ds} \\ v_{0s} \\ v'_{qr} \\ v'_{dr} \\ v'_{0r} \end{bmatrix} = \begin{bmatrix} r_s + \frac{p}{\omega_b}X_{ss} & \frac{\omega}{\omega_b}X_{ss} & 0 & \frac{p}{\omega_b}X_m & \frac{\omega}{\omega_b}X_m & 0 \\ \frac{\omega}{\omega_b}X_{ss} & r_s + \frac{p}{\omega_b}X_{ss} & 0 & \frac{\omega}{\omega_b}X_m & \frac{p}{\omega_b}X_m & 0 \\ 0 & 0 & r_s + \frac{p}{\omega_b}X_{is} & 0 & 0 & 0 \\ \frac{p}{\omega_b}X_m & (\frac{\omega-\omega_r}{\omega_b})X_m & 0 & r'_r + \frac{p}{\omega_b}X'_{rr} & (\frac{\omega-\omega_r}{\omega_b})X'_{rr} & 0 \\ -(\frac{\omega-\omega_r}{\omega_b})X_m & \frac{p}{\omega_b}X_m & 0 & -(\frac{\omega-\omega_r}{\omega_b})X'_{rr} & r'_r + \frac{p}{\omega_b}X'_{rr} & 0 \\ 0 & 0 & 0 & 0 & 0 & r_r \end{bmatrix} \begin{bmatrix} i_{qs} \\ i_{ds} \\ i_{0s} \\ i'_{qr} \\ i'_{dr} \\ i'_{0r} \end{bmatrix} \quad (13)$$

Where

$$X_{ss} = X_{Is} + X_M \quad (14)$$

$$X'_{rr} = X'_{Ir} + X_M \quad (15)$$

If $\omega = \omega_b$, the reference framework rotates at a speed of 120 p radians per second. An asynchronously synchronous reference frame is the term used to describe this frame. Following is an expression for the air gap flux connections ψ_{qm}, ψ_{dm}.

$$\psi_{qm} = L_m(i_{qs} + i'_{qr}) \quad (16)$$

$$\psi_{dm} = L_m(i_{ds} + i'_{dr}) \quad (17)$$

T_e can be shown as follows.

$$T_e = \frac{3}{2}\left(\frac{p}{2}\right)\left(\psi_{qm}i_{dr} - \psi_{dm}i_{qr}\right) \quad (18)$$

Since the stator resistance-related power loss is negligible, the following equations can be used to estimate electromagnetic power:

Active power is

$$(P_s) = (v_{ds}i_{ds} + v_{ds}i_{ds}) \quad (19)$$

The reactive power that the grid either injects/absorbs is calculated using the following equation.

$$Q_s = \left(v_{qs}i_{ds} - v_{ds}i_{qs}\right) \quad (20)$$

The electrical torque is illustrated as:

$$T_s = \psi_{dr}i_{qs} - \psi_{qr}i_{ds} \quad (21)$$

3. Structure and Modeling of ACR

When an overvoltage\current happens on the DCB or in the rotor windings, ACRs are meant to activate. The RSC is ignored and rendered inoperable when the ACR is activated (by stopping the power switches' pulses). By using the closed ACR switch to short-circuit the three-phase rotor winding, the DFIWG becomes a regular IM. Once a predetermined amount of time has passed or the

rotor current and DCBV have been restored to levels within their typical working range, the ACR can be detached and the RSC returned [46]-[48]. A three-phase rectifier and switch are used in the rotor ACR to link a resistor to the rotor winding. The switch is activated to prevent large currents from passing through the RSC but still allow them to pass through the rotor ACR resistor when the rotor currents get too high.

The rotor ACR action can often be represented as in (22). The parameters for each of the subsequent Eqs., are explained in detail [49], [50], [32]. The control strategy of the ACR system is depicted in Fig. 4.

$$V_C = F_S \, R_C \, I_C \tag{22}$$

The rotor's transient time constant is determined to be:

$$T_r{}^{SC} = \left(\frac{L_r{}^{SC}}{R_r + R_{\tau c}} \right) \tag{23}$$

The rotor current's highest level, which activates the ACR, is provided by:

$$I_r{}^{max} = \left(\frac{V_r{}^{max}}{\sqrt{(X_r{}^{sc})^2 + (R_{\tau c})^2}} \right) \tag{24}$$

The next estimate is used to determine the ACR resistance:

$$R_{\tau c} < \left(\frac{\sqrt{2} \, X_{rs}{}^{sc} \, V_r{}^{max}}{\sqrt{3.2 \, (V_s)^2 + 2(V_r{}^{max})^2}} \right) \tag{25}$$

The maximal allowed permissible rotor voltage, $V_r{}^{max}$, is calculated utilizing (26), which is provided in pu, and is dependent linearly on the DCV:

$$V_r = k \, m \, V_{DC} \, , and \; k = \left(\frac{1}{\sqrt{3}} \right) \frac{V_{DC}{}^{b}}{V_r{}^{b}} \tag{26}$$

The following represents the relationship between the charging function and the DCB of ACR:

$$V_r{}^{max} = IR_{DC} - V_{DC} = 0 \tag{27}$$

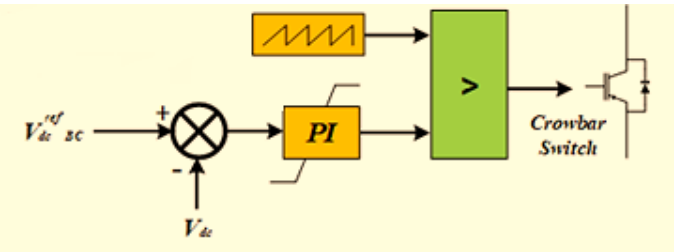

Fig. 4. Control of implemented crowbar system

4. Results and Discussions

Dynamic performance improvement of DFIWG under severe fault conditions is discussed in this work to show the role of the crowbar method. The system is tested in the case of the crowbar system and in its absence to show the benefit of adding it. The DFIWG parameters are studied such as (active and reactive power, generated current, angular speed, and DCBV) to show the impact of the proposed strategy on the machine performance. MATLAB/Simulink is used to simulate the examined DFIWG in order to confirm the efficacy of the suggested strategy. In this part, the FRTC

of the DFIWG is assessed via 100% voltage dip is assumed to occur as depicted in Fig. 5, and the DC link voltage transient responses under different crowbar resistances are analyzed. In addition, the simulated system parameters are listed in Table 2 [51]. The PI controller gains in this study are listed in the appendix.

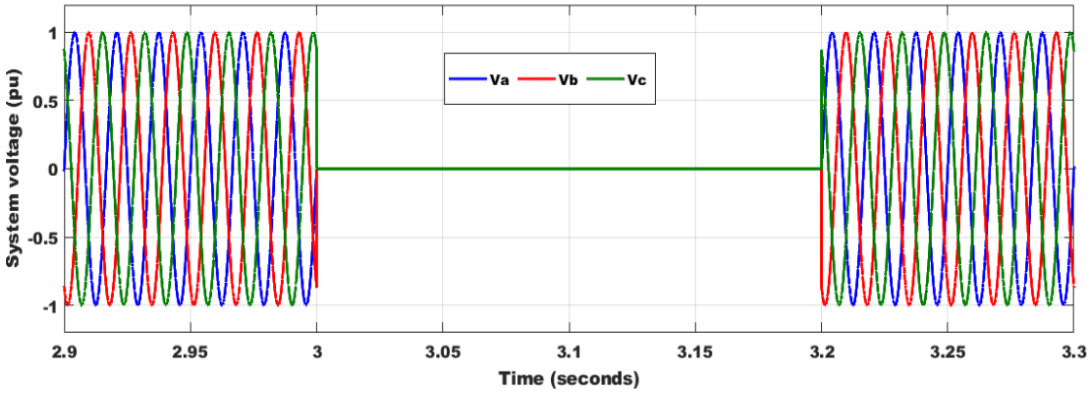

Fig. 5. System voltage

Table 2. Simulated DFIWG data

DFIWG parameters	Values
Rated power	1.5 MW
Rated stator voltage	575 V
Rated frequency	60 Hz
DC-Link voltage	1150 V
Pole pairs	3
Stator resistance	0.023 pu
Rotor leakage inductance	0.16 pu
Mutual inductance	2.9 pu
Stator leakage inductance	0.18 pu
Rotor resistance	0.016 pu
Inertia constant	0.685 pu

4.1. Case 1: Testing DFIWG in the Base Case Under 100% Voltage Dip

Achieving FRTC for DFIWG become an urgent need in recent years. One of the important techniques is the ACR which is still used in industry. Investigating the system without a crowbar is presented in Fig. 6. The system is tested under 100% voltage dip from 3 to 3.2 seconds to show the DFIWG parameters response. This hard situation leads to an increase in the generated current as in part (a), angular speed as in part (d), reactive power as in part (c), and DC bus voltage as in part (e) which increased to reach more than 4.3 pu, about 1.274 pu, about 1.07 Mvar, and about 2421 V, respectively as seen in Fig. 6. In contrast, this situation decreased the injected power to about zero MW as depicted in Fig. 6 (b). All of the obtained results are summarized in Table 3.

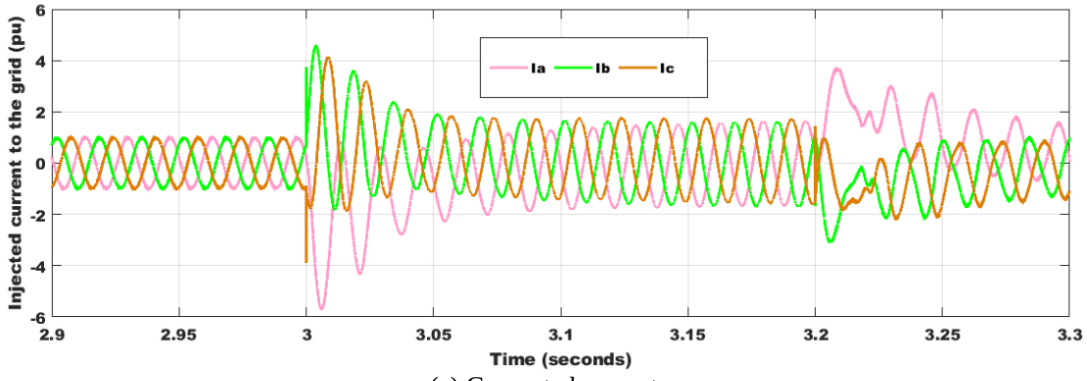

(a) Generated current

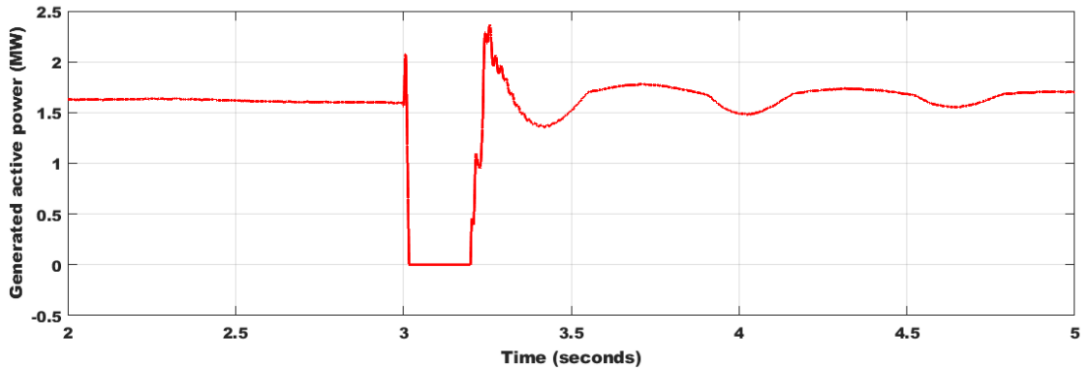

(b) Generated active power

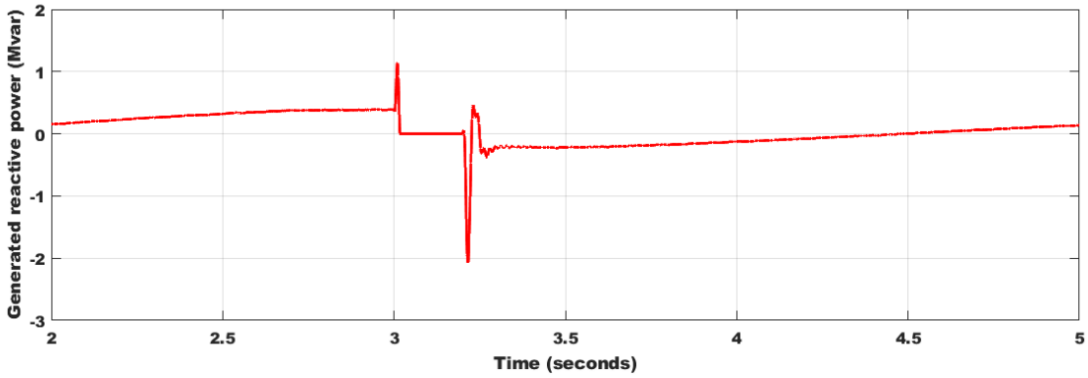

(c) Generated reactive power

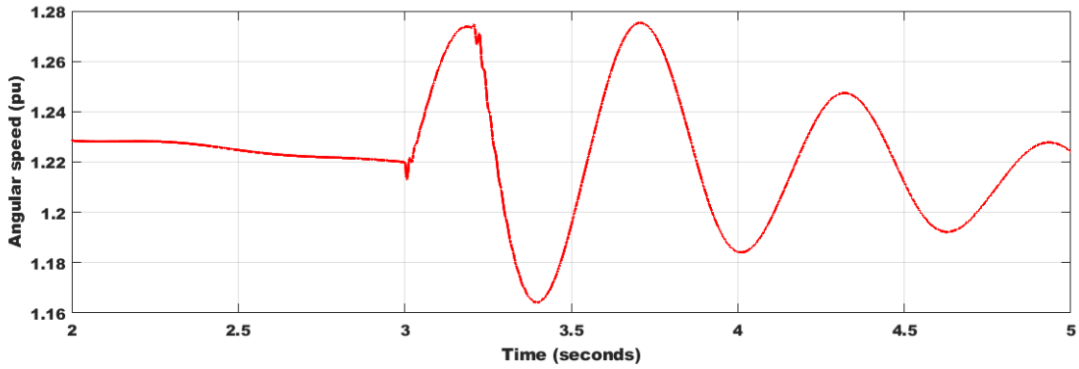

(d) Angular speed

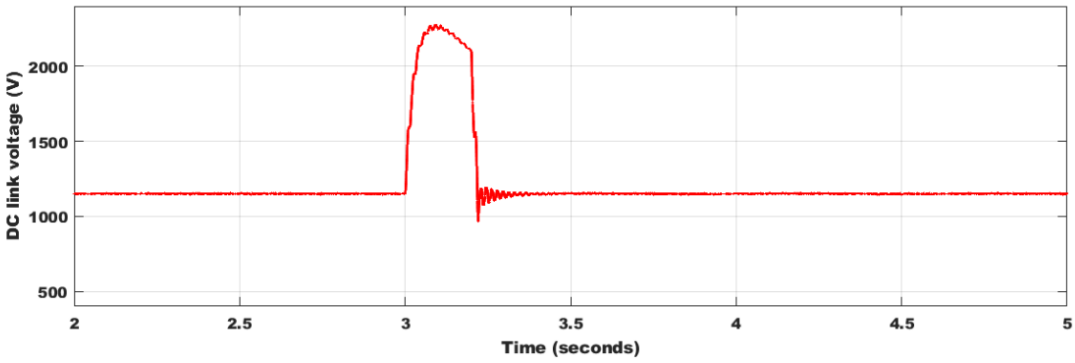

(e) DC link voltage

Fig. 6. System response in the base case under 100% voltage dip

4.2. Case 2: Testing DFIWG with Crowbar Under 100% Voltage dip

Investigating the system with a crowbar is presented in Fig. 7. The system is tested under 100% voltage dip from 3 to 3.2 seconds to show the DFIWG parameters response. This hard situation leads

to an increase in the generated current as depicted in (a), angular speed as depicted in (d), reactive power as depicted in (c), and DC bus voltage as depicted in (e), which increased to reach more than 4.1 pu, about 1.197 pu, about 1.09 Mvar, and about 1241 V, respectively as seen in Fig. 7. In contrast, this situation decreased the injected power to about zero MW as depicted in (b). The great effect of the crowbar appears on the DCBV which decreased by about 48.74%, and thus kept the converters from damage and helped in achieving FRTC. So, choosing the appropriate ACR value is important. All of the obtained results are summarized in Table 3.

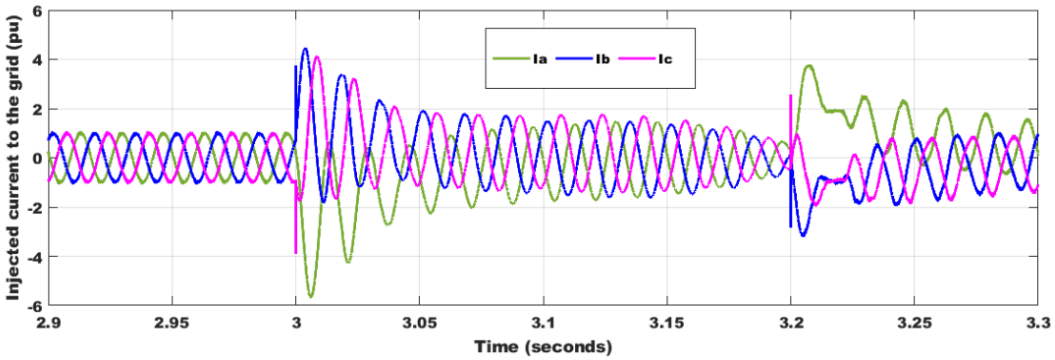

(a) Generated current

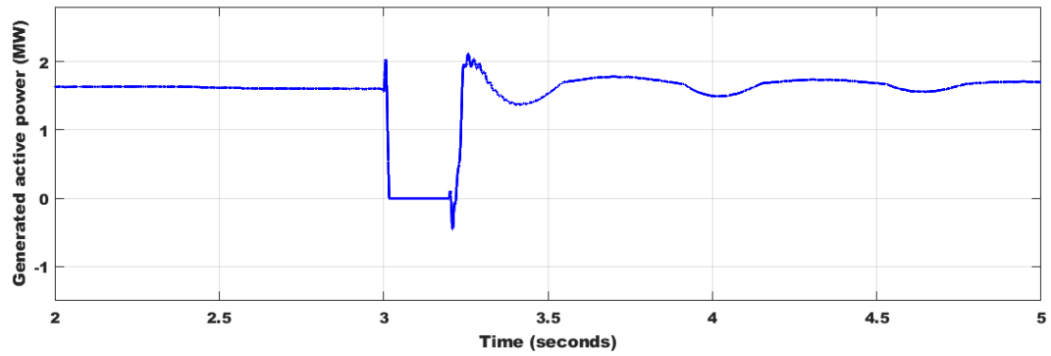

(b) Generated active power

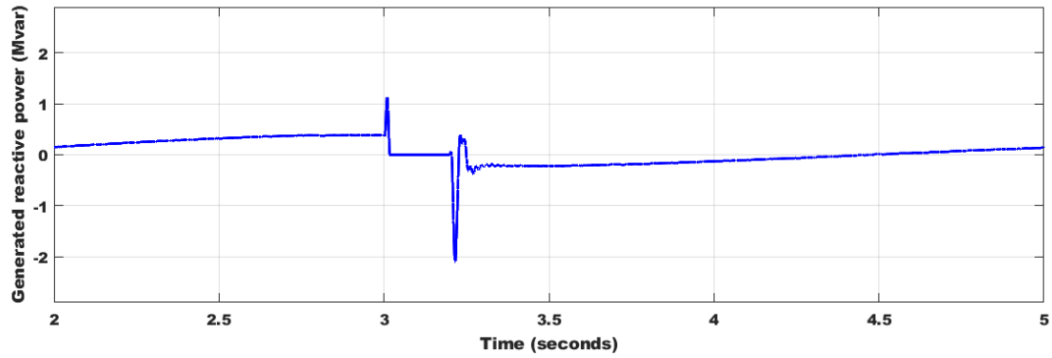

(c) Generated reactive power

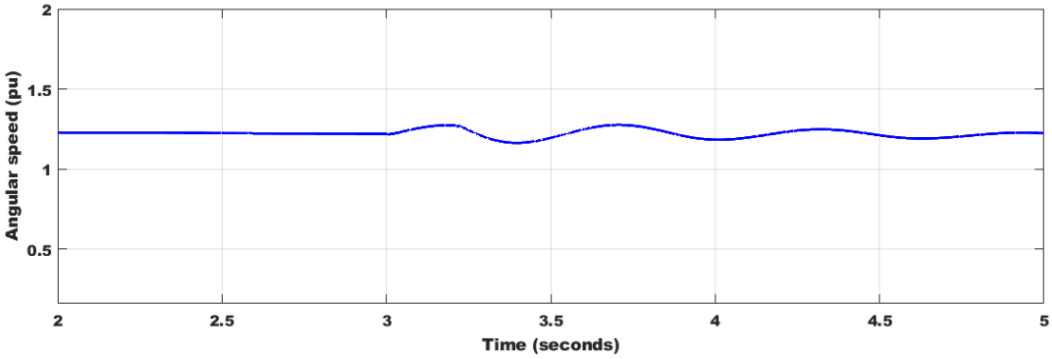

(d) Angular speed

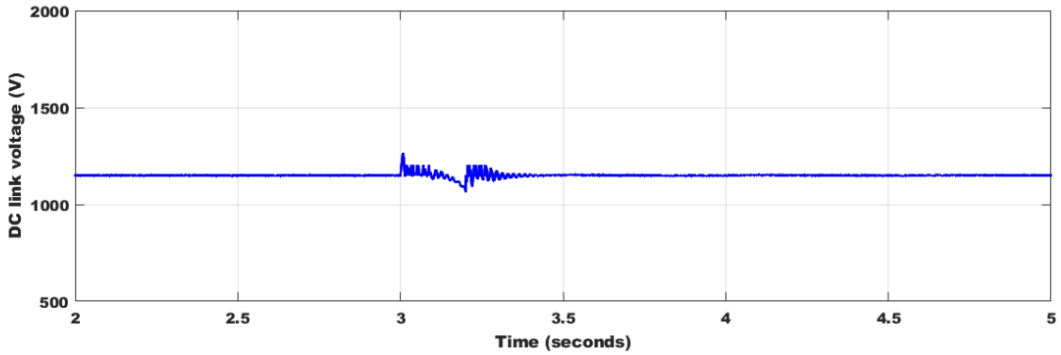

(e) DC link voltage

Fig. 7. System response in the case of using a crowbar under 100% voltage dip

Table 3. Summary of obtained results

Studied cases	Parameters
Without protection	Overvoltage at V_{DC} 2.11 pu P change ≈ (0 → 2.41) $\omega_r$change ≈ (1.17 → 1.27) Q change ≈ ((-2.07 → 1.06) I change (-5.84 → 4.17)
With crowbar	Overvoltage at V_{DC} 1.079 pu P change ≈ (-0.17 → 2.08) $\omega_r$change ≈ (1.15 → 1.197) Q change ≈ (-2.1 → 1.06) I change (-5.8 → 4.1)

The studied two cases showed the impact of the crowbar especially in the DCBV, which is the most important part of the machine, and without keeping it below the allowable limit (1.1 pu) will damage the machine or the protection system will force the DFIWG for tripping. So, choosing the appropriate resistance value of the crowbar deserves studying.

4.3. Case 3: Impact of Different Changing Crowbar Resistance Values on DCBV

The transient response of the DCBV at different resistance values under 100% voltage dip is investigated. Choosing the value of crowbar resistance is clearly important where it affects the machine's efficacy. It is chosen in the range of 10 times and 90 times larger rotor resistance to clarify the impact of this parameter. Fig. 8. shows the great effect of resistance value which means the value must be carefully chosen. The results show the value R=10Rr = 0.015 Ω decreases DCBV as seen in Fig. 8. The overvoltage at the V_{DC} reaches 2.11 pu, 1.572 pu, and 1.079 pu, respectively. These results showed that the DFIWG achieves FRTC only when R=10Rr.

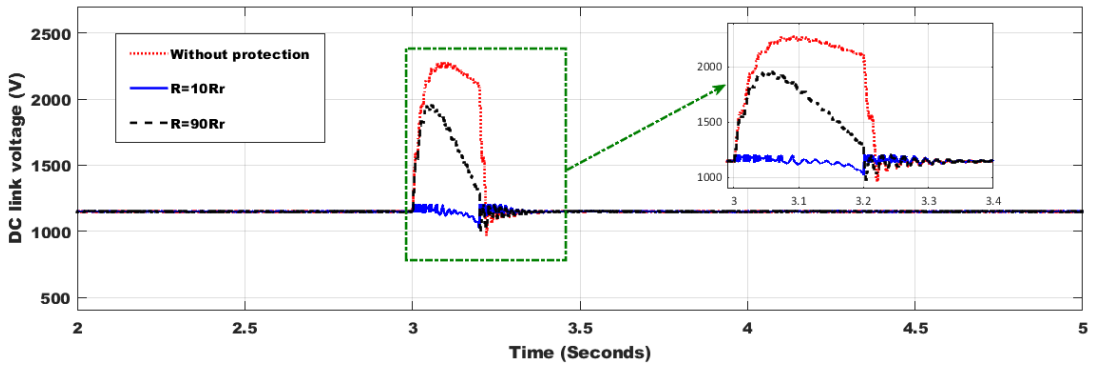

Fig. 8. The DCBV under different crowbar resistance values

5. Conclusions

In this study, FRTC is provided by proposing a planned control method for ACR performed in the VSC of the DFIWG. A drop in grid voltage causes the DCB to overvoltage, the winding to overcurrent, and P to decrease. The findings indicate that the ACR resistance value influences DCBV. For DCBV, the lowest value yields the best outcome. Therefore, when selecting a value, it must be high to avoid short circuit current and low for Vdc. The acquired findings have shown that using the suggested ACR in conjunction with the coordinated control technique can result in a significant improvement. The outcomes show that under fault situations, the DFIWG can be kept under control without disconnecting from the grid; consequently, the system can recover faster than it would have recovered in the absence of protection. The ACR not only dissipates the RE during fault conditions, but it also sets a limit on the RSC current value, protecting the RSC and reducing the destructive DCBV.

Author Contribution: All authors contributed equally to the main contributor to this paper. All authors read and approved the final paper.

Data Availability: The data used to support the findings of this study are available at reasonable request from the corresponding author.

Conflicts of Interest: The authors declare that they have no conflicts of interest.

Funding: This work has no external funding.

Appendix

Table 4. The PI controller gains in this study

RSC PI gains				GSC PI gains					
Voltage regulator (VR)		**Torque regulator (TR)**		**VR**		**VR**		**TR**		**VR**	
K_p = 7.9712	K_i = 0.0319	K_p = 2.7839	K_i = 0.0937	K_p = 0.2981	K_i = 97.278	K_p = 3	K_i = 0.02	K_p = 8	K_i = 500	K_p = 1.2	K_i = 5

References

[1] M. M. Mahmoud *et al.*, "Evaluation and Comparison of Different Methods for Improving Fault Ride-Through Capability in Grid-Tied Permanent Magnet Synchronous Wind Generators," *International Transactions on Electrical Energy Systems*, vol. 2023, no. 1, pp. 1-22, 2023, https://doi.org/10.1155/2023/7717070.

[2] M. M. Mahmoud *et al.*, "Voltage Quality Enhancement of Low-Voltage Smart Distribution System Using Robust and Optimized DVR Controllers : Application of the Harris Hawks Algorithm," *International Transactions on Electrical Energy Systems*, vol. 2022, no. 1, pp. 1-18, 2022, https://doi.org/10.1155/2022/4242996.

[3] A. M. Ewais, A. M. Elnoby, T. H. Mohamed, M. M. Mahmoud, Y. Qudaih, and A. M. Hassan, "Adaptive frequency control in smart microgrid using controlled loads supported by real-time implementation," *PLoS One*, vol. 18, no. 4, p. e0283561, 2023, https://doi.org/10.1371/journal.pone.0283561.

[4] M. A. Mostafa, E. A. El-Hay, and M. M. Elkholy, "An overview and case study of recent low voltage ride through methods for wind energy conversion system," *Renewable and Sustainable Energy Reviews*, vol. 183, p. 113521, 2023, https://doi.org/10.1016/j.rser.2023.113521.

[5] L. Rouco, K. Chan, J. Oesterheld and S. Keller, "Recent evolution of European grid code requirements and its impact on turbogenerator design," *2012 IEEE Power and Energy Society General Meeting*, pp. 1-9, 2012, https://doi.org/10.1109/PESGM.2012.6344819.

[6] M. Awad *et al.*, "A review of water electrolysis for green hydrogen generation considering

PV/wind/hybrid/hydropower/geothermal/tidal and wave/biogas energy systems, economic analysis, and its application," *Alexandria Engineering Journal*, vol. 87, pp. 213-239, 2024, https://doi.org/10.1016/j.aej.2023.12.032.

[7] L. Yang, G. Y. Yang, Z. Xu, Z. Y. Dong, K. P. Wong, and X. Ma, "Optimal controller design of a doubly-fed induction generator wind turbine system for small signal stability enhancement," *IET Generation, Transmission & Distribution*, vol. 4, no. 5, pp. 579-597, 2010, https://doi.org/10.1049/iet-gtd.2009.0553.

[8] M. M. Mahmoud, "Improved current control loops in wind side converter with the support of wild horse optimizer for enhancing the dynamic performance of PMSG-based wind generation system," *International Journal of Modelling and Simulation*, vol. 43, no. 6, pp. 952-966, 2023, https://doi.org/10.1080/02286203.2022.2139128.

[9] M. M. Mahmoud *et al.*, "Application of Whale Optimization Algorithm Based FOPI Controllers for STATCOM and UPQC to Mitigate Harmonics and Voltage Instability in Modern Distribution Power Grids," *Axioms*, vol. 12, no. 5, p. 420, 2023, https://doi.org/10.3390/axioms12050420.

[10] M. M. Mahmoud, M. Khalid Ratib, M. M. Aly, and A. M. M. Abdel-Rahim, "Wind-driven permanent magnet synchronous generators connected to a power grid: Existing perspective and future aspects," *Wind Engineering*, vol. 46, no. 1, pp. 189-199, 2022, https://doi.org/10.1177/0309524X211022728.

[11] M. Awad, M. M. Mahmoud, Z. M. S. Elbarbary, L. Mohamed Ali, S. N. Fahmy, and A. I. Omar, "Design and analysis of photovoltaic/wind operations at MPPT for hydrogen production using a PEM electrolyzer: Towards innovations in green technology," *PLoS One*, vol. 18, no. 7, p. e0287772, 2023, https://doi.org/10.1371/journal.pone.0287772.

[12] O. M. Kamel, A. A. Z. Diab, M. M. Mahmoud, A. S. Al-Sumaiti, and H. M. Sultan, "Performance Enhancement of an Islanded Microgrid with the Support of Electrical Vehicle and STATCOM Systems," *Energies*, vol. 16, no. 4, p. 1577, 2023, https://doi.org/10.3390/en16041577.

[13] M. M. Mahmoud, B. S. Atia, A. Y. Abdelaziz, and N. A. N. Aldin, "Dynamic Performance Assessment of PMSG and DFIG-Based WECS with the Support of Manta Ray Foraging Optimizer Considering MPPT, Pitch Control, and FRT Capability Issues," *Processes*, vol. 10, no. 12, p. 2723, 2022, https://doi.org/10.3390/pr10122723.

[14] A. H. Elmetwaly *et al.*, "Modeling, Simulation, and Experimental Validation of a Novel MPPT for Hybrid Renewable Sources Integrated with UPQC: An Application of Jellyfish Search Optimizer," *Sustainability*, vol. 15, no. 6, p. 5209, 2023, https://doi.org/10.3390/su15065209.

[15] C. Hamid, D. Aziz, O. Zamzoum, and A. El Idrissi, "Robust Control System for DFIG-Based WECS and Energy Storage in reel Wind Conditions," *EAI Endorsed Transactions on Energy Web*, vol. 11, pp. 1-6, 2024, https://doi.org/10.4108/ew.4856.

[16] Y. Li, Y. Zeng, J. Qian, F. Yang, and S. Xie, "Parameter Identification of DFIG Converter Control System Based on WOA," *Energies*, vol. 16, no. 6, p. 2618, 2023, https://doi.org/10.3390/en16062618.

[17] N. F. Ibrahim *et al*., "Operation of Grid-Connected PV System With ANN-Based MPPT and an Optimized LCL Filter Using GRG Algorithm for Enhanced Power Quality," *IEEE Access*, vol. 11, pp. 106859-106876, 2023, https://doi.org/10.1109/ACCESS.2023.3317980.

[18] M. Abdeen, M. Sayyed, J. L. Domínguez-García and S. Kamel, "Supplemental Control for System Frequency Support of DFIG-Based Wind Turbines," *IEEE Access*, vol. 10, pp. 69364-69372, 2022, https://doi.org/10.1109/ACCESS.2022.3185780.

[19] R. Hiremath and T. Moger, "Modified Super Twisting algorithm based sliding mode control for LVRT enhancement of DFIG driven wind system," *Energy Reports*, vol. 8, pp. 3600-3613, 2022, https://doi.org/10.1016/j.egyr.2022.02.235.

[20] H. Boudjemai *et al.*, "Application of a Novel Synergetic Control for Optimal Power Extraction of a Small-Scale Wind Generation System with Variable Loads and Wind Speeds," *Symmetry*, vol. 15, no. 2, p. 369, 2023, https://doi.org/10.3390/sym15020369.

[21] I. E. Maysse *et al*., "Nonlinear Observer-Based Controller Design for VSC-Based HVDC Transmission Systems Under Uncertainties," *IEEE Access*, vol. 11, pp. 124014-124030, 2023, https://doi.org/10.1109/ACCESS.2023.3330440.

[22] M. A. Chowdhury, G. M. Shafiullah, and S. M. Ferdous, "Low voltage ride-through augmentation of DFIG wind turbines by simultaneous control of back-to-back converter using partial feedback linearization technique," *International Journal of Electrical Power & Energy Systems*, vol. 153, p. 109394, 2023, https://doi.org/10.1016/j.ijepes.2023.109394.

[23] N. F. Ibrahim, A. Alkuhayli, A. Beroual, U. Khaled, and M. M. Mahmoud, "Enhancing the Functionality of a Grid-Connected Photovoltaic System in a Distant Egyptian Region Using an Optimized Dynamic Voltage Restorer: Application of Artificial Rabbits Optimization," *Sensors*, vol. 23, no. 16, p. 7146, 2023, https://doi.org/10.3390/s23167146.

[24] P. Verma, S. K, and B. Dwivedi, "Comprehensive investigation on doubly fed induction generator-Wind farms at fault ride through capabilities: technical difficulties and improvisations," *Energy Sources, Part A: Recovery, Utilization, and Environmental Effects*, pp. 1-33, 2021, https://doi.org/10.1080/15567036.2020.1857476.

[25] H. Boudjemai *et al*., "Experimental Analysis of a New Low Power Wind Turbine Emulator Using a DC Machine and Advanced Method for Maximum Wind Power Capture," *IEEE Access*, vol. 11, pp. 92225-92241, 2023, https://doi.org/10.1109/ACCESS.2023.3308040.

[26] A. Loulijat, M. El Marghichi, M. Makhad, and N. Ettalabi, "Crowbar With a Parallel RpLp Configuration Using PI Controller to Solve the Problem of DFIG-Wind Farm Stability During a Symmetrical Fault," *International Journal of Intelligent Engineering and Systems*, vol. 16, no. 6, pp. 799-812, 2023, https://doi.org/10.22266/ijies2023.1231.66.

[27] M. Liserre, R. Cárdenas, M. Molinas and J. Rodriguez, "Overview of Multi-MW Wind Turbines and Wind Parks," *IEEE Transactions on Industrial Electronics*, vol. 58, no. 4, pp. 1081-1095, 2011, https://doi.org/10.1109/TIE.2010.2103910.

[28] G. N. Sava, S. Costinas, N. Golovanov, S. Leva and D. M. Quan, "Comparison of active crowbar protection schemes for DFIGs wind turbines," *2014 16th International Conference on Harmonics and Quality of Power (ICHQP)*, pp. 669-673, 2014, https://doi.org/10.1109/ICHQP.2014.6842860.

[29] I. Ngom, A. B. Mboup, L. Thiaw, S. Skander-Mustapha and I. S. Belkhodja, "An improved control for DC-link fluctuation during voltage dip based on DFIG," *2018 9th International Renewable Energy Congress (IREC)*, pp. 1-6, 2018, https://doi.org/10.1109/IREC.2018.8362458.

[30] S. A. Saleh, A. S. Aljankawey, M. S. Abu-Khaizaran and B. Alsayid, "Influences of Power Electronic Converters on Voltage–Current Behaviors During Faults in DGUs—Part I: Wind Energy Conversion Systems," *IEEE Transactions on Industry Applications*, vol. 51, no. 4, pp. 2819-2831, 2015, https://doi.org/10.1109/TIA.2014.2387477.

[31] M. M. Altabbakh and L. T. Ergene, "Enhancement of the Low Voltage Ride Through Capability for Doubly Fed Induction Generator During Grid Voltage Dip," *2019 11th International Conference on Electrical and Electronics Engineering (ELECO)*, pp. 106-110, 2019, https://doi.org/10.23919/ELECO47770.2019.8990575.

[32] J. Yin, X. Huang, and W. Qian, "Analysis and research on short-circuit current characteristics and grid access faults of wind farms with multi-type fans," *Energy Reports*, vol. 11, pp. 1161-1170, 2024, https://doi.org/10.1016/j.egyr.2023.12.046.

[33] D. Zhu, X. Zou, S. Zhou, W. Dong, Y. Kang and J. Hu, "Feedforward Current References Control for DFIG-Based Wind Turbine to Improve Transient Control Performance During Grid Faults," *IEEE Transactions on Energy Conversion*, vol. 33, no. 2, pp. 670-681, 2018, https://doi.org/10.1109/TEC.2017.2779864.

[34] J. Mohammadi, S. Vaez-Zadeh, E. Ebrahimzadeh, and F. Blaabjerg, "Combined control method for grid-side converter of doubly fed induction generatorbased wind energy conversion systems," *IET Renewable Power Generation*, vol. 12, no. 8, pp. 943-952, 2018, https://doi.org/10.1049/iet-rpg.2017.0539.

[35] A. R. Nair, R. Bhattarai, M. Smith and S. Kamalasadan, "Parametrically Robust Identification Based Sensorless Control Approach for Doubly Fed Induction Generator," *IEEE Transactions on Industry Applications*, vol. 57, no. 1, pp. 1024-1034, 2021, https://doi.org/10.1109/TIA.2020.3035339

[36] M. Firouzi, M. Nasiri, S. Mobayen, and G. B. Gharehpetian, "Sliding Mode Controller-Based BFCL for Fault Ride-Through Performance Enhancement of DFIG-Based Wind Turbines," *Complexity*, vol. 2020,

no. 1, pp. 1-12, 2020, https://doi.org/10.1155/2020/1259539.

[37] M. R. Shafiee, H. S. Kartijkolaie, M. Firouzi, S. Mobayen, and A. Fekih, "A Dynamic Multi-Cell FCL to Improve the Fault Ride through Capability of DFIG-Based Wind Farms," *Energies*, vol. 13, no. 22, p. 6071, 2020, https://doi.org/10.3390/en13226071.

[38] B. Wadawa, Y. Errami, A. Obbadi, and S. Sahnoun, "Robustification of the H∞ controller combined with fuzzy logic and PI&PID-Fd for hybrid control of Wind Energy Conversion System Connected to the Power Grid Based on DFIG," *Energy Reports*, vol. 7, pp. 7539-7571, 2021, https://doi.org/10.1016/j.egyr.2021.10.120.

[39] H. Chojaa *et al.*, "Nonlinear Control Strategies for Enhancing the Performance of DFIG-Based WECS under a Real Wind Profile," *Energies*, vol. 15, no. 18, p. 6650, 2022, https://doi.org/10.3390/en15186650.

[40] F. Shiravani, J. A. Cortajarena, P. Alkorta, and O. Barambones, "Generalized Predictive Control Scheme for a Wind Turbine System," *Sustainability*, vol. 14, no. 14, p. 8865, 2022, https://doi.org/10.3390/su14148865.

[41] J. Liu, C. Wang, J. Zhao, B. Tan and T. Bi, "Simplified Transient Model of DFIG Wind Turbine for COI Frequency Dynamics and Frequency Spatial Variation Analysis," *IEEE Transactions on Power Systems*, vol. 39, no. 2, pp. 3752-3768, 2024, https://doi.org/10.1109/TPWRS.2023.3301928.

[42] R. Gianto, Purwoharjono, F. Imansyah, R. Kurnianto, and Danial, "Steady-State Load Flow Model of DFIG Wind Turbine Based on Generator Power Loss Calculation," *Energies*, vol. 16, no. 9, p. 3640, 2023, https://doi.org/10.3390/en16093640.

[43] N. F. Ibrahim *et al.*, "Multiport Converter Utility Interface with a High-Frequency Link for Interfacing Clean Energy Sources (PV\Wind\Fuel Cell) and Battery to the Power System: Application of the HHA Algorithm," *Sustainability*, vol. 15, no. 18, p. 13716, 2023, https://doi.org/10.3390/su151813716.

[44] U. Buragohain and N. Senroy, "Reduced Order DFIG Models for PLL-Based Grid Synchronization Stability Assessment," *IEEE Transactions on Power Systems*, vol. 38, no. 5, pp. 4628-4639, 2023, https://doi.org/10.1109/TPWRS.2022.3215125.

[45] M. M. Mahmoud *et al.*, "Integration of Wind Systems with SVC and STATCOM during Various Events to Achieve FRT Capability and Voltage Stability: Towards the Reliability of Modern Power Systems," *International Journal of Energy Research*, vol. 2023, no. 1, pp. 1-28, 2023, https://doi.org/10.1155/2023/8738460.

[46] S. A. E. M. Ardjoun, M. Denai, and M. Abid, "A robust power control strategy to enhance LVRT capability of grid-connected DFIG-based wind energy systems," *Wind Energy*, vol. 22, no. 6, pp. 834-847, 2019, https://doi.org/10.1002/we.2325.

[47] B. S. Atia *et al.*, "Applications of Kepler Algorithm-Based Controller for DC Chopper: Towards Stabilizing Wind Driven PMSGs under Nonstandard Voltages," *Sustainability*, vol. 16, no. 7, p. 2952, 2024, https://doi.org/10.3390/su16072952.

[48] S. R. K. Joga *et al.*, "Applications of tunable-Q factor wavelet transform and AdaBoost classier for identification of high impedance faults: Towards the reliability of electrical distribution systems," *Energy Exploration & Exploitation*, 2024, https://doi.org/10.1177/01445987241260949.

[49] A. M. A. Haidar, K. M. Muttaqi and M. T. Hagh, "A Coordinated Control Approach for DC link and Rotor Crowbars to Improve Fault Ride-Through of DFIG-Based Wind Turbine," *IEEE Transactions on Industry Applications*, vol. 53, no. 4, pp. 4073-4086, 2017, https://doi.org/10.1109/TIA.2017.2686341.

[50] Y. Ling, "A fault ride through scheme for doubly fed induction generator wind turbine," *Australian Journal of Electrical and Electronics Engineering*, vol. 15, no. 3, pp. 71-79, 2018, https://doi.org/10.1080/1448837X.2018.1525172.

[51] S. Swain and P. K. Ray, "Short circuit fault analysis in a grid connected DFIG based wind energy system with active crowbar protection circuit for ridethrough capability and power quality improvement," *International Journal of Electrical Power & Energy Systems*, vol. 84, pp. 64-75, 2017, https://doi.org/10.1016/j.ijepes.2016.05.006.